Geophysical Journal International

Geophys. J. Int. (2012) **191,** 765–780 doi: 10.1111/j.1365-246X.2012.05654.x

Combining HVSR microtremor observations with the SPAC method for site resonance study of the Tamar Valley in Launceston (Tasmania, Australia)

M. Claprood,[1,*] M. W. Asten[1] and J. Kristek[2]

[1]*School of Geosciences, Monash University, Melbourne VIC* 3800*, Australia. E-mail: Maxime.Claprood@ete.inrs.ca*

[2]*Faculty of Mathematics, Physics and Informatics, Comenius University, Mlynska dolina F1,* 842 48 *Bratislava, Slovak Republic and Geophysical Institute, Slovak Academy of Sciences, Dubravska cesta* 9, 845 28 *Bratislava, Slovak Republic*

Accepted 2012 August 15. Received 2012 June 7; in original form 2011 September 22

SUMMARY

The presence of the deep and narrow Tamar Valley in the City of Launceston (Tasmania, Australia), in-filled with soft sediments above hard dolerite bedrock, induces a complex pattern of resonance across the city. Horizontal to vertical spectrum ratio (HVSR) microtremor observations are combined with 1-D shear wave velocity (SWV) profiles evaluated from spatially averaged coherency spectra (SPAC) observations of the vertical component of the microtremor wavefield to complete a site resonance study in a valley environment such as the Tamar Valley. Using the methodology developed in a previous paper, 1-D SWV profiles are interpreted from observed coherency spectra (axial-COH) above the deepest point of the Tamar Valley, using pairs of sensors spatially separated parallel to the valley axis. The 1-D SWV profiles interpreted at five sites suggest the depth to bedrock interface varies from approximately $z = 25$ m north of the city, to $z = 250$ m above the deepest point of the valley. Numerical simulations of the propagation of surface waves in a 2-D model representation of the Tamar Valley compare well with HVSR observations recorded on two profiles transverse to the valley axis. HVSR observations can identify the in-plane shear (SV) frequency of resonance above the deepest part of the valley on two separate profiles transverse to the valley axis. By computing the ellipticity curves from the preferred SWV profiles interpreted by the SPAC method, the antiplane shear (SH) modes of resonance expected to develop in the Tamar Valley are identified; modes which HVSR observations alone fail to locate with precision. HVSR observations suggest a complex mix of 1-D and 2-D patterns of resonance develops across the valley. The results from this paper suggest that HVSR microtremor observations can be combined with SPAC microtremor method to characterize the geology and the pattern of resonance in a 2-D narrow structure such as the Tamar Valley.

Key words: Numerical solutions; Surface waves and free oscillations; Site effects; Wave propagation; Australia.

1 INTRODUCTION

The presence of low velocity sediments slows down the propagation of seismic waves generated by earthquake. It also induces amplification of the surface motion at a frequency of resonance proportional to the velocity and thickness of soft sediments above hard bedrock. Abrupt lateral variations of geology further amplify the surface motion and shift the frequency of resonance, generating a different pattern of resonance than expected above a layered earth. These local geology effects have significant importance when evaluating seismic hazard and seismic risk at specific sites (Horike 1985).

The situation of the City of Launceston (Tasmania, Australia) is an interesting example where such local geology effects are observed. While Launceston is not located in highly seismically active region (Fig. 1), damage has occurred to some buildings in the city from past earthquakes, which epicentres were located at more than 200 km from the city centre. Several hypotheses may explain the damages, including high vulnerability of the structure and complex pattern of resonance generated by abrupt changes in the near surface geology across the City of Launceston. While we do not discard the hypothesis of structure vulnerability, our study investigates the site resonance pattern expected to develop in the Tamar Valley.

The recording of ambient ground vibrations, or microtremors, has proven to provide a good estimation of the frequency of resonance and shear wave velocity (SWV) structure to complete such hazard

*Now at: Institut National de la Recherche Scientifique, Quebec City, QC, Canada.

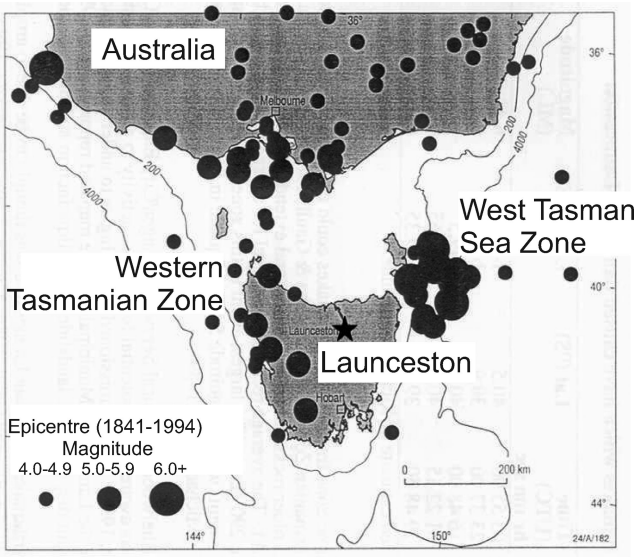

Figure 1. Location of Launceston in Tasmania, Australia. Epicentres of earthquakes with Richter magnitude of 4.0+ around Tasmania from 1884–1994 (modified from Michael-Leiba 1995).

zonation studies (Horike 1985; Field 1996; Kudo *et al.* 2002). For the purpose of this study, we use the term microtremor for ambient vibrations of any sources, from low frequency natural phenomena to high frequency human activities.

Single station microtremor methods, such as the horizontal to vertical spectrum ratio (HVSR) and the standard spectral ratio (SSR), are commonly used to estimate the frequency of resonance of layered earth geology, and to generate earthquake hazard or expected ground motion zonation maps (Ibs-von Seht & Wohlenberg 1999; Parolai *et al.* 2002; Fäh *et al.* 2003; Mirzaoglu & Dýkmen 2003; Tanimoto & Alvizuri 2006). The efficiency and low cost of HVSR field survey make that method a popular choice for resonance and microzonation studies (Lachet & Bard 1994). The interpretation of HVSR observations gives an accurate estimate of the fundamental frequency of resonance of soft sediments over hard bedrock (Field & Jacob 1995).

Different patterns of resonance develop above complex geologies such as 2-D and 3-D valleys in-filled with soft sediments. Several studies were completed to analyse the generation and propagation of the different components of surface waves induced in valleys of various dimensions (Bard & Bouchon 1980a,b, 1985; Kawase & Aki 1989; Frischknecht & Wagner 2004).

Many authors have demonstrated the potential of single station microtremor methods to detect a 2-D pattern of resonance, and to identify the frequencies of resonance expected to develop in a valley environment. Steimen *et al.* (2003) used the SSR method to analyse the resonance effects from the St Jakob-Tüllingen and Vetroz valleys in Switzerland. Results from the Vetroz Valley were studied in further detail by Roten *et al.* (2006) to better distinguish between laterally propagating surface waves induced by a 1-D pattern of resonance and vertically propagating standing waves generated by a 2-D pattern of resonance. Uebayashi (2003) used HVSR observations to constrain the modelling of 3-D basin structures; comparing modelled HVSR, observed HVSR and theoretical Rayleigh wave ellipticity curves to analyse the complex geology across the Osaka Basin (Japan). Hinzen *et al.* (2004) used HVSR observations to map the changes in sediments thickness across the normal fault Lower Rhine Embayment (Germany). Cara *et al.* (2008) noted significant variations in HVSR measurements from 90 sites above alluvial sediments in riverbeds in the city of Palermo (Italy). Recently, Lenti *et al.* (2009) analysed 2-D site amplification in the Nera River alluvial valley (Italy), using SSR and HVSR observations from microtremor and earthquake weak ground motion. Barnaba *et al.* (2010) used HVSR observations to estimate sediment thickness (assuming 1-D geology) in irregular shape valley in the Friuli region (Italy), comparing with gravity interpretation and seismic refraction velocity profiles.

We record HVSR observations in Launceston to analyse the frequencies of resonance in and around the Tamar Valley in Launceston. The choice of the HVSR method rather than SSR was justified on the basis that HVSR observations do not require the use of a reference station on hard bedrock, whereas the distant location for a reference station relative to the other stations can violate the hypothesis of spatial stationarity of the microtremor wavefield.

Single station microtremor observations do not provide good estimates of the SWV structure of a soil (Asten *et al.* 2002; Chávez-García *et al.* 2007), an important parameter to evaluate for site hazard study. Several authors demonstrated that the reliability of site resonance studies is greatly improved by combining array based and single station microtremor observations to evaluate the SWV structure and the pattern of resonance. For example, Satoh *et al.* (2001) used HVSR observations at 48 sites to constrain SWV profiles evaluated by array based FK method at four sites in the Taichung Basin (Taiwan). Scherbaum *et al.* (2003) used the FK method to evaluate dispersion curves to constrain the velocity to depth dependence, and HVSR observations to constrain the layer thickness in the Lower Rhine Embayment (Germany). Parolai *et al.* (2005) proposed a joint inversion of HVSR and velocity dispersion curves, using fundamental and higher modes of propagation to determine the SWV structure by a genetic algorithm at a test site in the Cologne area (Germany). Similarly, using microtremor observations at four sites in the cities of Kushiro, Odawara, and Tokyo (Japan), Arai & Tokimatsu (2005) demonstrated that a joint iterative non-linear inversion of HVSR spectra and array derived velocity dispersion curves gives better results at evaluating SWV profiles than using velocity dispersion curves alone. Di Giulio *et al.* (2006) combined HVSR and FK observations in the Colfiorito Basin (Italy) to derive SWV profiles. Chávez-García *et al.* (2007) conducted a microzonation study of the city of Colima (Mexico) by combining HVSR observations at 315 sites with array based ReMi and spatially averaged coherency spectra (SPAC) microtremor methods at eight sites for improved resolution. Roten & Fäh (2007) concluded that the combined inversion of velocity dispersion curves obtained from the FK method, with 2-D frequencies of resonance evaluated from SSR observations, was a reliable method to evaluate SWV profile to bedrock interface in the Rhône Valley.

Several authors have analysed the use of array based microtremor methods in complex geology. For example, Cornou *et al.* (2003a,b) used the MUSIC algorithm with HVSR observations to identify the wavefield associated with site amplification in the Grenoble Valley (France), using an extensive array of 29 three-component seismometers with a total array aperture of 1 km. Hartzell *et al.* (2003) used the FK and MUSIC methods to detect edge generated surface waves with a dense array of 52 sensors in the Santa Clara Valley (USA), using site response spectra from earthquake generated motion to evaluate the SWV profile. Roten *et al.* (2006, 2008) used the FK method to identify the modes of resonance expected to develop in the Rhône Valley (Switzerland). Seismic noise tomography was used by Picozzi *et al.* (2009) to image shallow structural heterogeneities with an array of 21 geophones at the Nauen test site in Germany.

In this study, we present the results of a site resonance study conducted in and at the edge of the Tamar Valley in Launceston, combining the results obtained from HVSR and SPAC observations at separate sites. Until recently, the use of SPAC method was restricted to regions where the geology could be approximated by a layered earth geology. A methodology was developed in Claprood *et al.* (2011), paper subsequently referred to as CAK1, to permit the use of temporally averaged coherency spectra observations to evaluate SWV profile above the deepest point of a valley. Building on the results obtained in CAK1 at two sites DBL and RGB, we complete the site resonance study in Launceston by analysing SPAC observations at three additional sites (GUN, OGL, and KPK) to evaluate 1-D SWV profiles in and outside the valley. HVSR observations at all five sites are analysed to constrain SPAC observations and to evaluate the frequencies of resonance at separate sites in Launceston. Additional HVSR observations are recorded on two profiles transverse to the valley axis to identify the different modes of resonance which develop in the Tamar Valley.

2 GEOPHYSICAL SETTINGS

While other causes such as structure vulnerability are not excluded, we investigate the possibility that site amplification response due to local geology effects could induce the earthquake damages observed in Launceston. Information on the geology of Launceston is available from unpublished maps from Mineral Resources Tasmania, borehole logs held by the Launceston City Council, and a gravity survey completed by Leaman (1994). The geological map of Launceston presented in Fig. 2 outlines the rapid changes in surface geology in the Central Business District of Launceston, with the geological interpretation of two gravity profiles recorded across the valley.

The area covered by this survey is topographically flat. The bedrock comprises dense, fractured and weathered Jurassic dolerite; which provides reduced seismic risk and excellent foundation conditions (Leaman 1994). It is covered by poorly consolidated materials, i.e. clays, sands, conglomerates, silts and fills which can be compressible, water saturated, plastic, and of low density. Quaternary alluvial sediments (silts, gravels, fills) were deposited in valleys floor and other marshy areas near sea level. These sediments have poor cohesion, negligible strength, and may be thixotropic. The ancient valley systems beneath Launceston are Tertiary rift valleys, filled with low density Tertiary sands and clays. A gravity interpretation (Leaman 1994) identified two palaeo-valley systems, i.e. the Trevallyn-Tamar lineament referred as the Tamar Valley in this paper, and the North Esk Palaeovalley, both trending in a NNW-SSE direction. The Tamar Valley is the focus of our research for it is more continuous and better defined than the North Esk Valley. Interpretation of the gravity survey indicates that the Tamar Valley has a width of 700 to 1000 m and an approximate maximum depth of 250 m.

Borehole logs, located at proximity to site DBL and in the northern part of Launceston (Inveresk, Fig. 2), are drilled to a maximum depth of 20 m, hitting hard dolerite bedrock in Inveresk only. The boreholes drilled at site DBL were terminated, for unknown reason, at depth less than 10 m in silty sand, interpreted to be the interface between Quaternary and Tertiary sediments. The interpretation of borehole logs gives little information about the geology inside the Tamar Valley. While the interpretation of the gravity survey from Leaman (1994) provides some knowledge about the extent of the soft sediments filling the Tamar Valley, it adds little information about the shear wave velocity inside the valley.

3 GEOPHYSICS SURVEYS

Prior to the first microtremor field survey completed in October 2006, some geophysical surveys have been completed to characterize the geology and to identify the frequency of resonance at several sites in Launceston. We briefly present the main conclusions interpreted from a gravity survey (Leaman 1994) and a microzonation project (Michael-Leiba 1995), which results suggested the need of acquiring additional microtremor observations in Launceston.

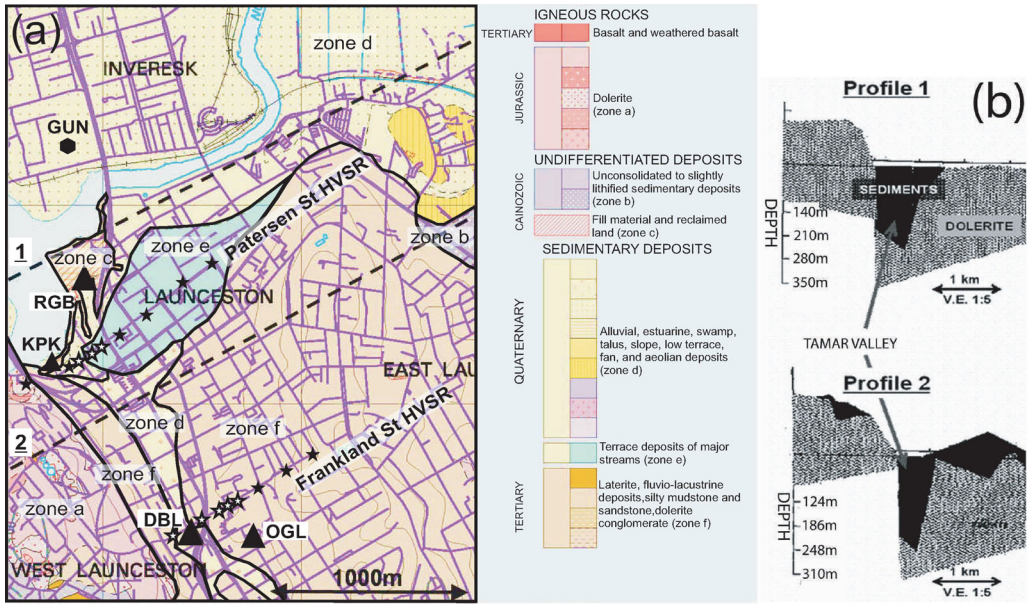

Figure 2. (a) Map of surface geology of Launceston (modified from Mineral Resources Tasmania), divided into six zones by thick black lines. Triangles and hexagons are location of SPAC microtremor observations at sites GUN, RGB, KPK, DBL and OGL. Black stars: stations for HVSR profiles. White stars: projected stations for HVSR profiles. Dashed lines: location of two gravity profiles from Leaman (1994) which geological interpretation is presented on panel (b).

3.1 Gravity survey

The geological interpretation of two gravity profiles recorded across the city is presented in Fig. 2(b). The survey provided some evaluation of the geometry of the valley systems, and outlined the importance to complete a microzonation study in the city of Launceston to evaluate the frequency of resonance at separate sites in the city. We use this interpretation to constrain some SWV profiles recorded in Launceston, and to constrain the geometry of the Tamar Valley during the numerical simulations.

3.2 Microzonation project

The microzonation study was completed by Michael-Leiba (1995), by recording HVSR observations to estimate the natural period of resonance at 56 sites in Launceston. The observations were used to create two zoning maps of the city, depicting site soil factors and building height groups which may be affected by resonance.

The periods of resonance evaluated during this microzonation project present a large range of values (0.1–1.5 s), variations which do not always appear to fit the interpreted bedrock interface from gravity data (Leaman 1994). The hypothesis of multiple layering of sediments, non-uniformity of the layer with respect to shear-wave velocity, or departure from simplified layered earth geology were advanced by Michael-Leiba (1995) to explain these disagreements. We further investigate the hypothesis that 2-D effects generated by the presence of soft sediments in the Tamar Valley could explain some of these contradictory observations.

4 SITE RESONANCE STUDY

We recorded array based SPAC and single station HVSR microtremor observations in and around the Tamar Valley to increase our knowledge of the pattern of resonance which develops in Launceston.

Two HVSR profiles transverse to the valley axis are used to identify the frequencies of resonance which are induced in the Tamar Valley. The SPAC method is used to evaluate the SWV structure above the deepest point of the valley, which is used to compute the Rayleigh wave ellipticity curve. The peak of the ellipticity curve is an estimation of the expected frequency of resonance f_h when assuming a layered earth geology. Using a model developed by Bard & Bouchon (1985), we compute the frequencies of all expected modes of resonance in the Tamar Valley using the SWV information from SPAC interpretation and the frequencies of resonance observed from the HVSR profiles. Both sets of observations (SPAC and HVSR) are needed to complete the site resonance study of the Tamar Valley because: (1) HVSR observations can not resolve for all modes of resonance, and (2) the modes of resonance computed from the SWV determined by the SPAC method need validation from HVSR profiles at different points across the valley. Numerical simulations of the propagation of surface waves in a 2-D model representation of the Tamar Valley are completed to confirm the interpretation of microtremor observations recorded in Launceston, and to better define the geometry, geology, and modes of resonance of the valley.

4.1 SPAC method

The SPAC method was introduced by Aki (1957) under the name spatial autocorrelation method. Assuming the spatial and temporal stationarity of microtremors, coherency spectra are evaluated between all pairs of sensors in an array. The spatially averaged coherency spectrum $C(f)$ is computed for multiple inter-station separations as:

$$C(f) = J_0(kr) = J_0\left[\frac{2\pi f r}{V(f)}\right], \quad (1)$$

where J_0 is the Bessel function of first kind and zero order, k is the spatial wavenumber at frequency f, r is the interstation separation, and $V(f)$ is the S-wave velocity dispersion function of a layered earth model, which SWV profile is evaluated (Aki 1957; Okada 2003; Asten 2006a). While Aki (1957), Fäh *et al.* (2007), and Köhler *et al.* (2007) demonstrated the potential of using vertical and horizontal components of the microtremor wavefield (method referred as the 3cSPAC), the vertical component alone is used in this project for its simpler processing. Observed coherency spectra are directly fit to theoretical coherency spectrum (COH) by least-square optimization (Herrmann 2002) to evaluate the SWV to depth profile, as proposed by Asten *et al.* (2004). The domain of validity of the frequency interval to interpret SPAC observations with an array of sensors is still debated in the literature (Henstridge 1979; Okada 2006; Asten 2006a,b; Ekström *et al.* 2009). We select the interval of valid frequencies on a case-by-case scenario from the analysis of the microtremor wavefield. The valid frequency range is identified on each selected sites on the coherency spectra.

When the hypothesis of a layered earth is not valid, suggesting the presence of 2-D effects from the valley, we use the methodology developed in CAK1 to identify the patterns of resonance and evaluate 1-D SWV profiles from microtremor observations recorded in a valley environment. The coherency spectra observed with pairs of sensors with separation parallel to the valley (axial-COH) of the vertical component alone is fit to the theoretical coherency spectrum to evaluate the depth to bedrock interface above the deepest point of the valley. The use of single pair of sensors to evaluate the coherency spectrum, replacing the spatial averaging by temporal averaging and increasing the length of the microtremor time series, has been validated by different studies (Aki 1957; Capon 1973; Morikawa *et al.* 2004; Chávez-García *et al.* 2005; Claprood & Asten 2010).

4.2 HVSR method

The HVSR, introduced by Nogoshi & Igarashi (1971) and popularized by Nakamura (1989), provides a good estimate of the natural frequency of resonance of soft sediments over hard bedrock (f_h). In a layered earth geology, the HVSR peak is empirically found to be a reliable estimation of the Rayleigh wave ellipticity R_0 (Lachet & Bard 1994; Tokimatsu 1997; Scherbaum *et al.* 2003), where the shape of the elliptical motion is determined by the shear wave frequency of resonance in particular, and more generally by the elastic parameters of the earth. In a typical interpretation sequence, Rayleigh wave ellipticity curves are computed from the SWV profiles evaluated by the SPAC method. At the shear wave frequency of resonance of an assumed layered earth, the Rayleigh wave's elliptical motion tends to degenerate into a dominantly horizontal motion (Asten *et al.* 2002), showing a peak on the ellipticity curve.

An intricate pattern of resonance develops across a valley infilled with low velocity sediments. Surface waves bounce back and forth from the edges of the valley, creating interference and inducing a pattern of resonance different than that expected over a layered geology. A 2-D pattern of resonance develops in deep and narrow valleys. A critical shape ratio was expressed by Bard & Bouchon (1985) to better define the conditions of formation of 1-D and

2-D patterns of resonance with respect to the dimensions of the valley. The shape ratio of a valley is defined as the ratio between the maximum thickness of sediments H to the half-width w of the basin (the length over which the local sediments thickness is greater than half the maximum thickness H).

Different modes of resonance develop in a valley, shifting the frequency of resonance to higher frequencies when compared to its equivalent layered geology. Bard & Bouchon (1985) recognized the SH mode of resonance excited by the axial component of horizontal motion (parallel to the valley axis), and the SV and P modes of resonance excited by the transverse component of horizontal motion (perpendicular to the valley axis) and the vertical component of motion. The theoretical SH and SV modes of resonance are expected at frequencies:

$$f_{mn}^{\mathrm{SH}} = f_h \sqrt{(2m+1)^2 + (n+1)^2 \frac{H^2}{w^2}}, \tag{2}$$

$$f_{\mathrm{fund}}^{\mathrm{SV}} = f_h \sqrt{1 + \left(\frac{2.9H}{w}\right)^2}, \tag{3}$$

where f_h is the frequency of resonance of an equivalent layered earth, m and n are the number of nodes in the vertical and horizontal standing modes, respectively. By decomposing the horizontal microtremor time series into its axial and transverse components of motion relative to the valley axis, we seek to detect these theoretical frequencies of resonance on HVSR observations recorded in the Tamar Valley in Launceston. At a qualitative level, a difference in observed HVSR frequency maxima for axial and transverse components of motion can be an indicator of 2-D effects in the geology. Where the different frequency maxima are resolvable, we are able to make quantitative conclusions on the nature of a 2-D valley.

5 MICROTREMOR OBSERVATIONS

Microtremor observations were recorded in October 2006 and 2007 in the city centre of Launceston. We used seven vertical component Mark L28—4.5 Hz cut-off frequency sensors to record SPAC observations; and one three-component Mark L4C—1 Hz cut-off frequency geophone to record HVSR observations at the centre of each array during the 2006 field survey. Two 5 min time series were recorded at each site. To gain sensitivity at depth, we used four three-component Guralp CMG-3ESP—30 and 60 s period geophones to record SPAC and HVSR observations in 2007. Observations were recorded with time series of 20 to 30 min, sufficient to ensure reliability in the observed coherency spectra computed with a limited number of sensors (Chávez-García & Rogríguez 2007; Chávez-García *et al.* 2007; Claprood & Asten 2010) and to significantly reduce the statistical variability of microtremor observations (Picozzi *et al.* 2005).

The time series are divided into 80-s time segments, with 50 per cent overlap, weighted with a Hanning bell, and fast-Fourier transformed in the frequency domain to obtain the raw spectra $S_i(f)$ of microtremor energy at every sensor i. HVSR or SPAC processing were then computed on every time segment, from which the temporal average over all time segments was evaluated.

The SPAC results for sites DBL and RGB have been used in CAK1 to develop the methodology permitting the use of the SPAC method in valley environment. We now include three additional sites (KPK, GUN, OGL), integrating HVSR data with the SPAC data for identifying perturbations attributable to the 2-D geology. The location of the sites GUN, RGB, KPK, DBL and OGL is presented in Fig. 2(a). Two HVSR profiles are also recorded transverse the Tamar Valley along Paterson and Frankland Streets to analyse the frequencies of resonance across the valley.

5.1 SPAC observations

The complex coherency spectrum $C_{ij}(f)$ between each pair of sensors (i, j) is computed using the equation:

$$C_{ij}(f) = \frac{S_i(f)\, S_j^*(f)}{\sqrt{S_i(f)\, S_i^*(f)\, S_j(f)\, S_j^*(f)}}, \tag{4}$$

where $*$ denotes complex conjugate. Complex coherency spectra are averaged over all time segments to yield the temporally averaged coherency spectrum at each pair of sensors. The abbreviation COH is used for coherency spectrum throughout this paper. SPAC are computed by averaging over azimuth for all interstation separations possible from the array geometry. We used centred hexagonal arrays of $n = 6$ sensors during the 2006 field survey and centred triangular arrays of $n = 3$ sensors during the 2007 field survey. The geometry of both arrays is presented in Fig. 3.

The coherency spectra observed at all five sites in Launceston are presented in Fig. 4 for all pairs of sensors of selected interstation separations, along with the spatially averaged coherency spectra recorded at five sites in Launceston and the theoretical coherency spectrum computed from the preferred SWV profile at each site.

Coherency spectra were recorded with two centred hexagonal arrays of 15 and 30 m radius at site GUN. The SWV profile was evaluated by fitting the theoretical coherency spectra to the observed SPAC for frequencies $1.5 \leq f \leq 7.0$ Hz. The observed SPAC agree well with the theoretical coherency spectra, and the SWV profile evaluated compares well with the borehole logs obtained from the Launceston City Council.

The site RGB is located above the eastern flank of the Tamar Valley. Previous analysis of SPAC observations at site RGB in CAK1 suggested a directionality of the microtremor wavefield (Claprood & Asten 2010), which was not induced by 2-D resonance from the Tamar Valley (CAK1).

The site KPK is assumed to be located above the deepest point of the valley (Leaman 1994). Observed coherency spectra at site KPK are analysed over an extended frequency interval ($2.5 \leq f \leq 12.0$ Hz) with a 28 m radius centred hexagonal array in 2006 and two 28 m radius centred triangular arrays in 2007. The bedrock interface is not detected with SPAC observations alone due to the small array size; HVSR and gravity interpretation were used as constraints to fix the depth to bedrock interface at site KPK.

The site DBL is assumed to be located above the deepest point of the Tamar Valley at approximately 1 km southeast of site KPK. A 20 m radius centred hexagonal array was used in 2006 to resolve the shallow layers (Claprood & Asten 2008a). This site was

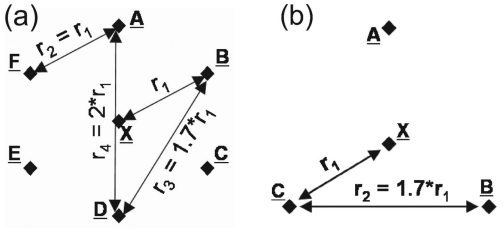

Figure 3. Common SPAC array geometries. (a) Centred hexagonal array of six stations with four interstation separations r_1, r_2, r_3 and r_4. (b) Centred triangular array of three stations with two interstation separations r_1, r_2.

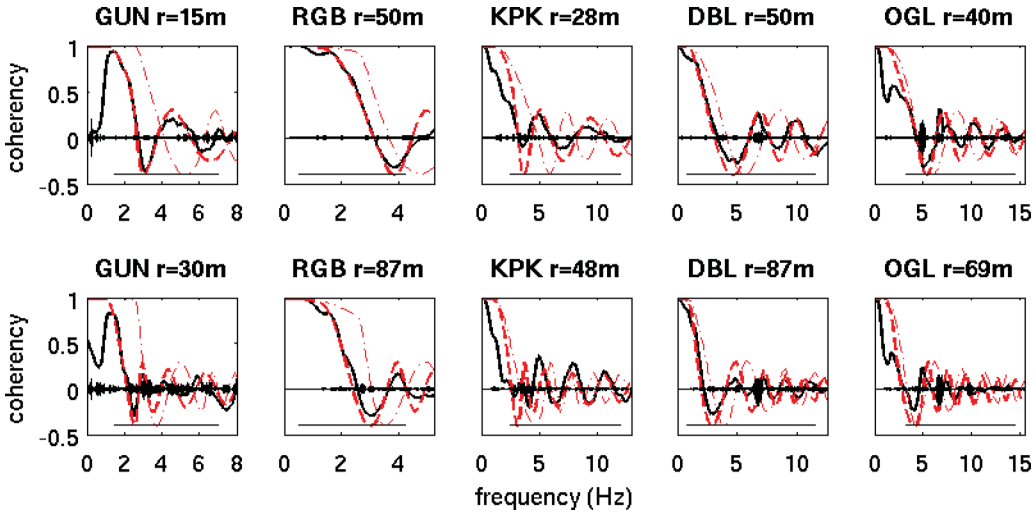

Figure 4. Best-fit coherency models at five sites for selected interstation separations. Hexagonal arrays used at sites GUN and KPK, sum of two triangle arrays with pair of sensors XA oriented axial and transverse to valley axis used at sites RGB, DBL and OGL. Thick black curve is real component of observed spatially averaged coherency spectrum (COH). Bars are roughened imaginary component of observed COH. Thick dashed red curve is the theoretical COH for the fundamental mode Rayleigh wave, for the preferred SWV layered earth model. Dash–dotted red curve is the theoretical COH for the 1st higher mode Rayleigh wave. Straight line at bottom of each graph shows the frequency interval over which the theoretical COH is fitted to the observed COH.

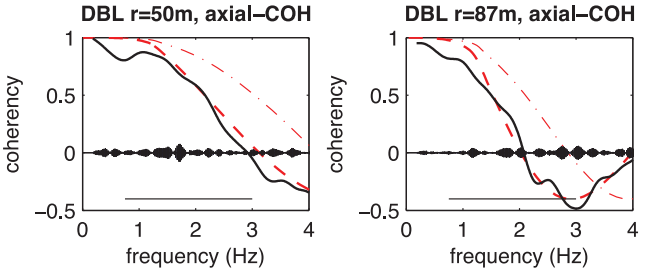

Figure 5. Best-fit coherency model at site DBL between theoretical coherency spectrum (thick dashed red curve for fundamental mode, dash–dotted red curve for 1st higher mode) and observed axial-COH (thick black curve) for interstation separations $r_1 = 50$ m and $r_2 = 87$ m on frequency interval $0.75 \leq f \leq 3.0$ Hz.

revisited in 2007 with two 50 m radius centred triangular arrays for improved resolution at depth. As outlined in CAK1, different behaviours were detected on the coherency spectra observed at low frequencies with the 50 m radius array with respect to azimuth. Following the methodology developed in CAK1 concerning the use of the SPAC method in a valley environment, only the axial-COH was used to evaluate the depth to bedrock interface at site DBL. The coherency spectra observed on other pairs of sensors are affected by the 2-D resonance pattern, and could not be used to interpret a 1-D SWV profile at site DBL. Fig. 5 presents the fit between the theoretical coherency spectra and observed axial-COH at site DBL for interstation separations $r_1 = 50$ m and $r_2 = 87$ m on the frequency interval $0.75 \leq f \leq 3.0$ Hz.

Observed coherency spectra at site OGL, located on the eastern flank of the Tamar Valley, show poor resolution at low frequency, and were used in combination with HVSR observations to resolve the bedrock interface at this site. The depth to bedrock of the SWV profile was adjusted so the peak of the ellipticity curve, computed from SPAC observations, would match the frequency of resonance observed on HVSR data.

Conversely to Di Giulio *et al.* (2012) who explored the whole model space by ranking the best classes of models for the inversion of surface-wave dispersion inversion, we only present the preferred SWV profiles (thick lines) and the 20 per cent lower and upper bounds in sediments thickness (dashed lines) evaluated at all five sites (Fig. 6). We believe our approach is sufficient to analyse and differentiate the impact of the complex geology such as the Tamar Valley on SPAC and HVSR observations. Fig. 6 outlines the variability in the shear wave velocity structures interpreted at different locations within the city of Launceston. The bedrock interface is interpreted to be at $z \simeq 25$ m at site GUN, and deeper than 200 m at sites KPK and DBL (Fig. 6). This explains the large range of periods of resonance recorded by Michael-Leiba (1995) over the city. The interpreted 1-D SWV profiles are used to compute the expected frequencies of resonance at these five separate sites in Launceston.

5.2 HVSR observations

Horizontal to vertical spectrum ratios are computed to estimate the frequency of resonance at separate sites in Launceston. The sensors are oriented to record the horizontal components parallel and perpendicular to the valley axis to identify the f^{SH} and f^{SV} frequencies of resonance which develop in a valley (Bard & Bouchon 1985; Steimen *et al.* 2003; Roten *et al.* 2006). We use the term axial-HVSR for HVSR computed with the axial horizontal component to the valley axis, and to the term transverse-HVSR for HVSR computed with the transverse horizontal component. For the example of a valley striking north-south, we compute HVSR as:

$$\mathrm{HVSR} = \frac{\sqrt{S_{\mathrm{NS}}^2 + S_{\mathrm{EW}}^2}}{S_{\mathrm{UP}}}, \tag{5}$$

$$\mathrm{axial-HVSR} = \frac{S_{\mathrm{NS}}}{S_{\mathrm{UP}}}, \tag{6}$$

$$\mathrm{transverse-HVSR} = \frac{S_{\mathrm{EW}}}{S_{\mathrm{UP}}}, \tag{7}$$

where S_{NS} is the north-south (axial in Launceston) component of horizontal power spectrum, S_{EW} is the east-west (transverse in Launceston) component of horizontal power spectrum, and S_{UP} is the vertical microtremor power spectrum.

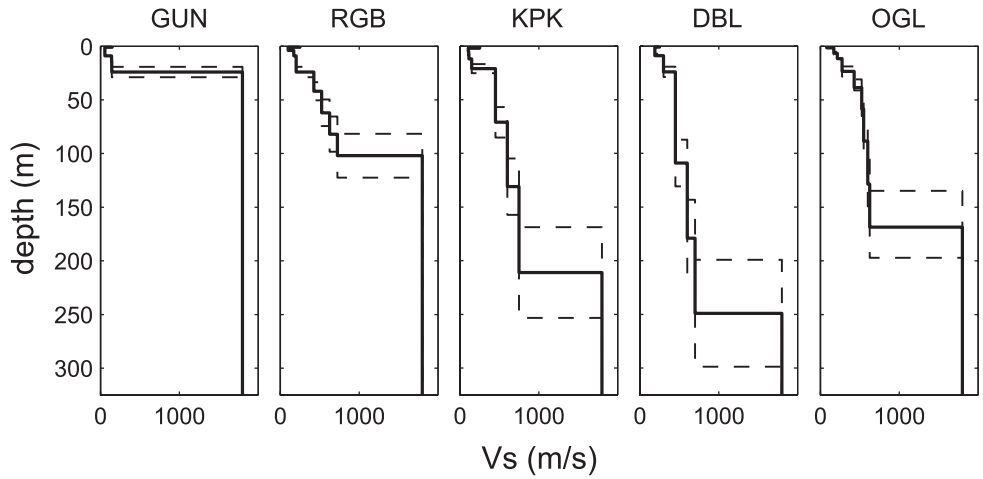

Figure 6. Thick lines: preferred SWV profiles evaluated at at sites GUN, RGB, KPK, DBL and OGL from SPAC observations. Dashed lines: lower and upper bounds on sediment thickness of preferred SWV profiles by adjusting layers thickness by ±20 per cent.

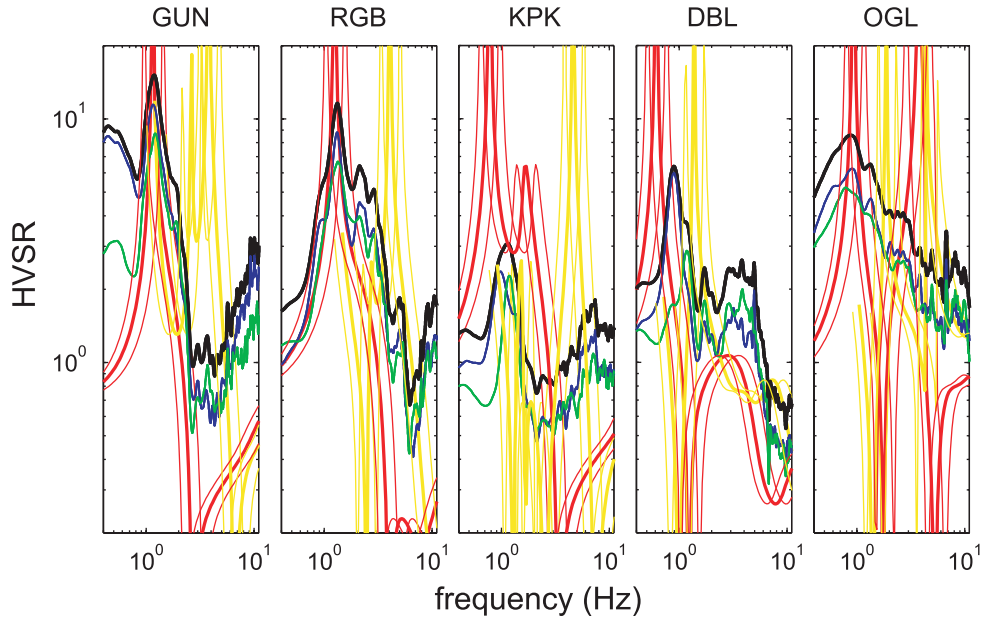

Figure 7. HVSR observations at all five sites. Thick black solid line is conventional HVSR; blue line is axial-HVSR; green line is transverse-HVSR; thick red and yellow lines are Rayleigh wave ellipticity curve of fundamental mode R_0 and first higher mode R_1 from the preferred SWV profile at each site; thin red and yellow lines are R_0 and R_1 from the lower and upper bounds of SWV profiles.

We present HVSR observations recorded at the centre sensor of all SPAC arrays in Fig. 7. HVSR observations are compared to the Rayleigh wave ellipticity computed from the 1-D SWV profiles evaluated at all sites (Fig. 6).

Different behaviours are observed on the HVSR curves depending on the site analysed. Conventional, axial and transverse-HVSR all agree well with the Rayleigh wave ellipticity curves computed at sites GUN, RGB and OGL. A sharp peak is recognized on HVSR observations at $f_h = 1.18$ Hz at site GUN, and at $f_h = 1.31$ Hz at site RGB. It is interesting to note the frequency of resonance is lower at site GUN than at site RGB, despite a much shallower bedrock interface (SWV profiles, Fig. 6). Sediments of very low velocity at site GUN are thought to be the main cause of such a low frequency of resonance. The frequency of resonance is estimated at $f_h = 0.87$ Hz from HVSR observations at site OGL.

Despite the fact that the sites RGB and OGL are assumed to be located within the Tamar Valley, they do not show 2-D frequencies of resonance. We propose the hypothesis that the east flank of the valley is dipping at such low angle that the geology can be approximated by a layered earth for microtremor studies at these sites. This hypothesis of a layered earth does not hold true above the deepest point of the valley, where a separation of the modes of resonance is observed at sites KPK and DBL. At both sites, the peaks are located at different frequencies on axial-HVSR and transverse-HVSR; at higher frequency than the expected frequency of resonance f_h computed from the ellipticity curve from SPAC observations by considering a layered earth. Fig. 8 better expresses that difference by zooming on the HVSR curves at sites KPK and DBL around their frequencies of resonance.

The difference in behaviour observed on the axial and transverse-HVSR is typical of the separation of modes of resonance expected in deep and narrow valleys. The frequencies of resonance $f_{01}^{\mathrm{SH}} = 0.90$ Hz on the axial-HVSR and $f_{\mathrm{fund}}^{\mathrm{SV}} = 1.16$ Hz on the transverse-HVSR at site KPK; and $f_{01}^{\mathrm{SH}} = 0.90$ Hz and $f_{02}^{\mathrm{SH}} = 1.20$ Hz on the

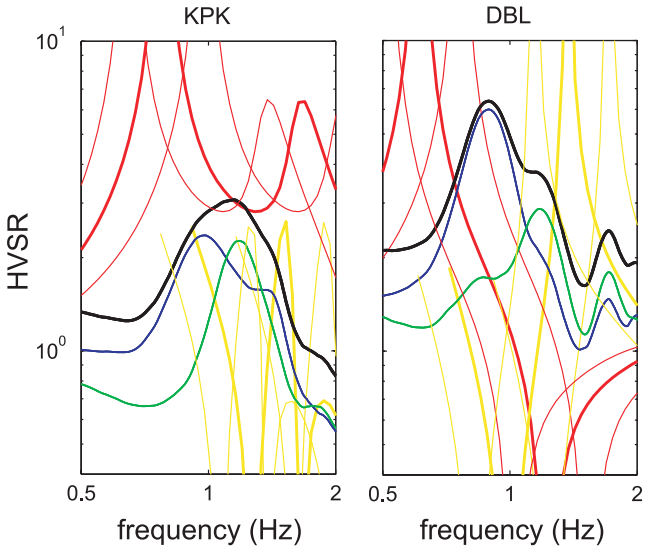

Figure 8. HVSR observations at sites KPK and DBL around the frequencies of resonance. Same legend as Fig. 7.

axial-HVSR, and $f^{SV}_{fund} = 1.18$ Hz on the transverse-HVSR at site DBL were identified in Claprood & Asten (2008b).

We observe that the uncertainty in the 1-D SWV profiles can not explain the discrepancy observed between the ellipticity curves and HVSR observations at sites KPK and DBL. A significant change in the sediment thickness can not explain the separation in the frequency of resonance regarding to the orientation of the horizontal components. Similar analysis is also true concerning the higher modes of propagation, which affect both horizontal components by the same amount. This is not observed on HVSR curves, where the horizontal components are shifted differently depending on their orientation.

6 TAMAR VALLEY CHARACTERIZATION

Building on the SPAC and HVSR results obtained at five separate sites, we complete the site characterization study of the Tamar Valley by recording two HVSR profiles transverse to the valley axis. The first profile runs along Paterson Street, at proximity to the sites KPK and RGB, while the second profile runs along Frankland Street at proximity to the sites DBL and OGL (Fig. 2a).

Axial- and transverse-HVSR profiles are constructed by presenting the observed HVSR curves side by side with respect to the distance from the western edge of the valley. A grey tone contour map is generated from the traditional HVSR observations. Each HVSR curve is normalized so its peak is fixed to a value of 1. This normalization was completed to present a smoother map of HVSR observations, and to better observe the variations in the pattern of resonance across the Tamar Valley. It is commonly accepted that, while HVSR observations are reliable to evaluate the frequency of resonance, their amplitude does not give an accurate estimation of the actual site amplification (Lachet & Bard 1994; Dravinski *et al.* 1996), which justifies the normalization process.

6.1 Paterson Street HVSR profile

The Paterson Street profile is formed from HVSR observations recorded at different sensors at site KPK and additional stations along Paterson Street. The axial-HVSR and transverse-HVSR profiles on Paterson Street are presented in Figs 9 and 10.

Combining all geophysical information (gravity interpretation, SPAC and HVSR), we evaluate the geometry of the valley along Paterson Street profile. The maximum depth to the bedrock interface is fixed at $H = 230$ m from gravity interpretation (Leaman 1994). The width at half-depth is evaluated at $w = 500$ m to match most observed HVSR peaks to the expected frequencies of resonance of modes SH and SV. These expected frequencies of resonance are computed by the Bard and Bouchon's model using the ellipticity curve from SPAC observations. A shape ratio of $SR = 0.46$ is computed for the Tamar Valley along Paterson Street. The expected frequencies of resonance of modes SH and SV are annotated on Figs 9 and 10.

The peak on the axial-HVSR profile on Paterson Street is located at $f = 0.90$ Hz. This is significantly higher than the expected frequency of resonance for an equivalent layered earth ($f_h = 0.74$ Hz), and is located between the expected $f^{SH}_{00} = 0.82$ Hz and $f^{SH}_{01} = 1.01$ Hz frequencies of resonance. A double peak feature is observed at

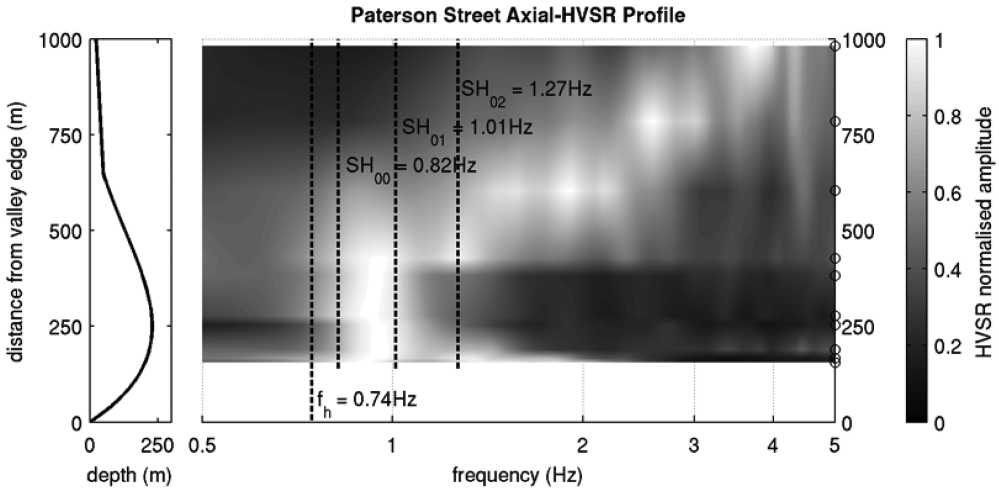

Figure 9. Observed axial-HVSR profile recorded across the Tamar Valley along Paterson Street. The contour map shows amplitude of HVSR (white is maximum) as a function of position and frequency. Expected frequencies of resonance f_h from Rayleigh wave ellipticity at site KPK, and f^{SH}_{00}, f^{SH}_{01}, and f^{SH}_{02} computed from Bard and Bouchon's model (eq. 2) are shown as vertical dashed lines. Circles on the right are the location of HVSR observations along the profile. Left: model representation of the Tamar Valley along Paterson Street used in the numerical simulations.

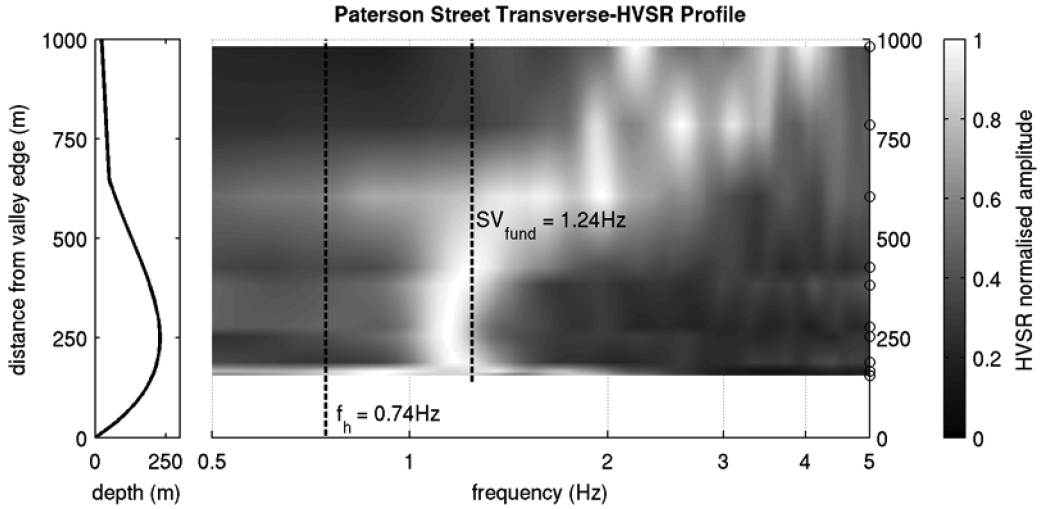

Figure 10. Observed transverse-HVSR profile recorded across the Tamar Valley along Paterson Street. Expected frequencies of resonance f_h from Rayleigh wave ellipticity at site KPK, and $f^{\mathrm{SV}}_{\mathrm{fund}}$ computed from Bard and Bouchon's model (eq. 3) are presented. Left: model representation of the Tamar Valley along Paterson Street used in the numerical simulations.

$f = 1.27$ Hz on axial-HVSR and on the transverse-HVSR profile (Fig. 10). We suggest this peak corresponds to a 1-D frequency of resonance above the flank of the valley. A 1-D frequency of resonance was identified at $f_h = 1.31$ Hz from HVSR observations at site RGB which is located at similar distance to the edge of the valley, supporting this hypothesis. Such complex spectral resonance in a valley environment, including a mix of 1-D and 2-D patterns of resonance, has been recognized by Lenti *et al.* (2009). The peak located at $f = 1.16$ Hz above the deepest point of the valley at $x = 250$–300 m on the transverse-HVSR profile on Paterson Street (Fig. 10) agrees well with the expected $f^{\mathrm{SV}}_{\mathrm{fund}} = 1.24$ Hz computed from Bard and Bouchon's model.

6.2 Frankland Street HVSR profile

HVSR observations recorded at selected sensors from the SPAC arrays at sites DBL and OGL and additional stations are used to construct this HVSR profile across the Tamar Valley, located approximately 1 km southeast of the Paterson Street profile. The HVSR stations from the site OGL are projected parallel to the valley axis to correctly evaluate the distance from each station perpendicular to the edge of the valley. The profile contains a total of ten stations, unequally spaced. Figs 11 and 12 present the Frankland Street axial-HVSR and transverse-HVSR profiles. An expected 1-D frequency of resonance of $f_h = 0.61$ Hz is evaluated on the ellipticity curve computed from SPAC observations at site DBL. The peaks identified on HVSR profiles in Figs 11 and 12 are clearly located at higher frequencies.

Combining the SWV profiles obtained by the SPAC method and observed frequencies of resonance observed on HVSR data is necessary to evaluate the geometry of the valley along this profile. The maximum sediments thickness is evaluated at $H = 250$ m from axial-COH interpretation at site DBL while the numerical simulations of the valley presented in the Section 6.3 allows to determine the width at half-depth ($w = 421$ m) by fitting the expected and observed frequencies of resonance from HVSR profiles.

We observe a peak at $f = 0.90$ Hz on the axial-HVSR profile above the deepest point of the valley in Fig. 11. This frequency

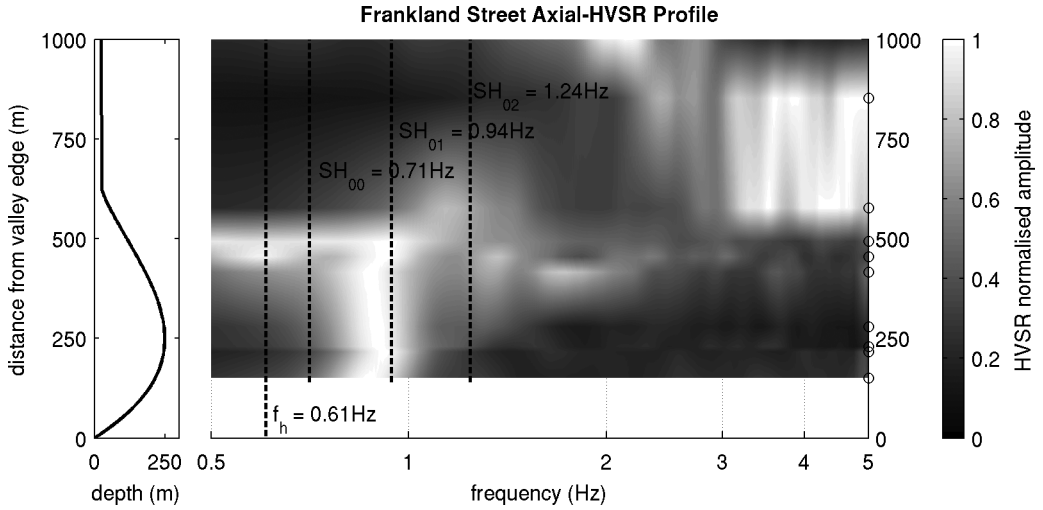

Figure 11. Observed axial-HVSR profile recorded across the Tamar Valley along Frankland Street. Left: model representation of the Tamar Valley used in numerical simulations.

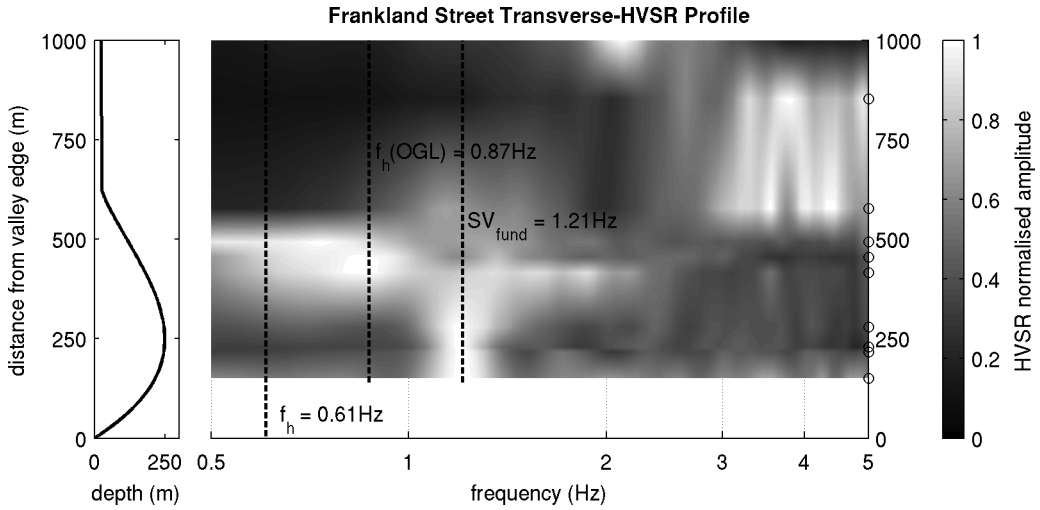

Figure 12. Observed transverse-HVSR profile recorded across the Tamar Valley along Frankland Street. Left: model representation of the Tamar Valley from numerical simulations.

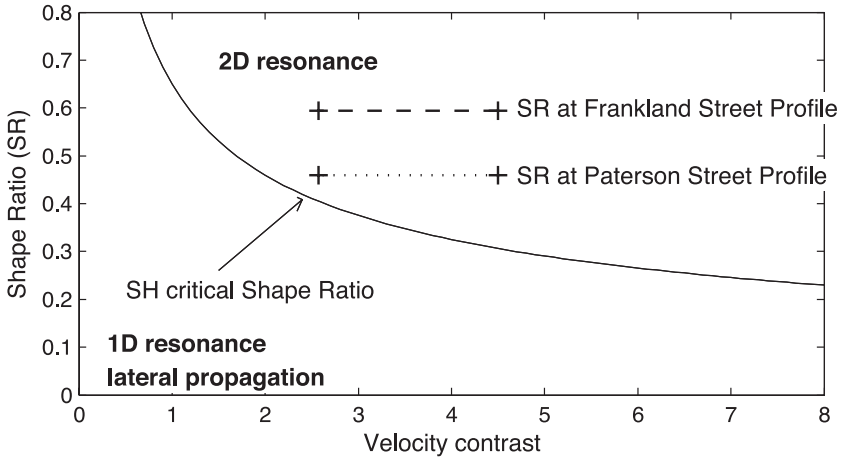

Figure 13. Shape ratio (SR) computed for the Tamar Valley in function of velocity contrast along Frankland Street Profile (dashed line with crosses, $H = 250$ m, $w = 421$ m, for $SR = 0.59$), and along Paterson Street Profile (dotted line with crosses, $H = 230$ m, $w = 500$ m, for $SR = 0.46$). Velocity contrast is computed between bedrock velocity (1800 m s^{-1}) and minimum (400 m s^{-1}) and maximum (700 m s^{-1}) Tertiary sediments velocity from the SWV profiles evaluated at site DBL and KPK. Solid curve is the critical shape ratio of SH mode of resonance in function of velocity contrast (from Bard & Bouchon 1985).

approximately equals that of the computed $f_{01}^{\mathrm{SH}} = 0.94$ Hz. SH modes of resonance of higher order could not be detected on the axial-HVSR profile.

On the transverse-HVSR profile (Fig. 12), a clear peak is identified at frequency $f = 1.18$ Hz above the deepest point of the valley, which corresponds to the expected frequency of resonance $f_{\mathrm{fund}}^{\mathrm{SV}} = 1.21$ Hz. This peak, along with the peak observed on axial-HVSR at $f = 0.90$ Hz (Fig. 11), suggests the presence of a 2-D pattern of resonance above the deepest part of the Tamar Valley.

A peak is also identified at location $x = 450$ m above the gently dipping flank of the valley, which location corresponds to the site OGL. A 1-D frequency of resonance was previously identified at $f_h = 0.87$ Hz on HVSR observations and the ellipticity curve computed from the preferred SWV profile at site OGL. This suggests the resonance behaviour above this side of the valley reacts as a layered earth geology; in a similar pattern than was previously observed on the HVSR profile along Paterson Street.

We note a significant change in the pattern and frequencies of resonance on the axial- and transverse-HVSR profiles at $x \simeq 500$ m. HVSR data show a peak at constant frequency $f \simeq 3.5$ Hz on both profiles for $x > 550$ m. This suggests the geology east of the Tamar Valley can be approximated by a layered earth.

Fig. 13 presents the shape ratio of the valley computed along Paterson and Frankland Street profiles. The shape ratios computed on both profiles are plotted against the critical shape ratio of the SH mode of resonance in Fig. 13. It shows that a 2-D pattern of resonance is expected to develop in the Tamar Valley along both profiles when considering the SH mode of resonance, which confirms the results obtained with HVSR observations. The velocity contrast was computed for a dolerite bedrock shear wave velocity estimated at 1800 m s^{-1}, and Tertiary sediments shear wave velocity of 400 to 700 m s^{-1}, evaluated on the 1-D SWV profiles at sites KPK and DBL.

6.3 Numerical simulations

We simulate the propagation of surface waves in complex geology to constrain the geometry and geology of the Tamar Valley. We use the program package NOISE developed within the European 5FP project 'Site Effects Assessment using Ambient

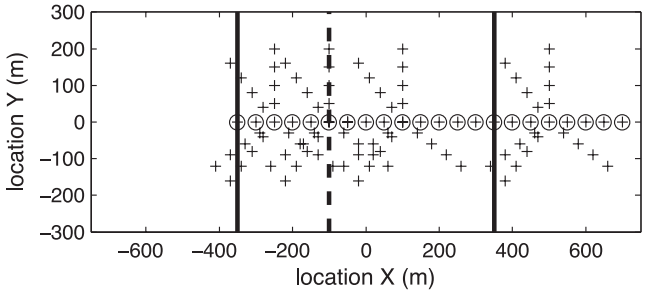

Figure 14. Location of all simulated receivers across the Tamar Valley. Crosses: receivers forming SPAC arrays. Circles: receivers for HVSR profile across the valley. Thick vertical solid lines are the edges of the valley. Thick vertical dashed line is the axis of the valley, at its deepest point.

Excitations (SESAME)' to complete the numerical simulations (Moczo & Kristek 2002). NOISE is designed to compute the propagation of seismic noise (microtremors) in 3-D heterogeneous geological structures with a planar free surface, from surface and near-surface random sources (Moczo & Kristek 2002). The package is divided in two main programs: Ransource for the random space-time generation of microtremor point sources and Fdsim for the computation of seismic wavefields in 3-D heterogeneous geological structures based on the finite-difference method (Moczo *et al.* 2002; Kristek *et al.* 2002, 2006; Moczo *et al.* 2007).

The 2-D model representation of the Tamar Valley is described in CAK1, to which the reader is referred to for additional information concerning the initial parameters used in the numerical simulations. We only model the Frankland Street profile because SPAC observations recorded above the deepest point of the valley along the Paterson Street profile (site KPK) do not offer adequate resolution of the depth to bedrock interface, an important constraint in the numerical simulations. Simulated three-component microtremor time series are recorded at a series of receivers positioned at 50 m spacing to construct a HVSR profile across the model representation of the valley (circles in Fig. 14). Additional simulated receivers were also positioned to record simulated SPAC data used in CAK1 (crosses in Fig. 14).

The parameters of the model representation of the Tamar Valley are determined to fit HVSR and SPAC microtremor observations recorded along the Frankland Street profile. The SWV profile used in the simulations above the deepest point of the valley is an approximation of the SWV profile evaluated by the axial-COH method at site DBL (Fig. 15b). The geometry of the right flank of the valley is constrained by simulating HVSR measurements over a layered earth model, varying the depth to bedrock interface to fit SPAC and HVSR observations at site OGL, and HVSR observations at different stations on the Frankland Street profile. The SWV profile interpreted at site OGL, and its approximation used in the numerical simulations are presented in Fig. 15(c). The assumption of a layered earth on this flank of the valley is postulated by the behaviour of HVSR observations presented in Section 6.2.

The 2-D model representation of the valley (Fig. 15a) is simulated by an exponential analytical expression inspired from Paolucci (1999), which parameters are described in CAK1. A layered earth with depth to bedrock $z = 25$ m is interpreted right of the valley from the HVSR profiles presented in Figs 11 and 12. The propagation of surface waves in a layered earth geology using the SWV profile above the deepest point of the Tamar Valley model (Fig. 15b) is also simulated to better understand the differences between HVSR observations in a layered earth and in a 2-D valley.

6.4 Simulated HVSR

Simulated HVSR curves are computed at all points across the valley. These are used to validate the frequencies of resonance which develop within the valley, and the variations of HVSR observations along the Frankland Street profile.

HVSR simulated at ten receivers are presented in Fig. 16. The top left panel presents the HVSR curves simulated for the equivalent layered earth, with the Rayleigh wave ellipticity curve computed from the SWV profile of Fig. 15(b). HVSR simulated at different locations across the valley are presented in the other panels with respect to the distance x to the left edge of the valley. The deepest point of the valley is located at $x = 250$ m.

We observe some variability in the HSVR curves simulated above a layered earth and those simulated at different locations across the 2-D model representation of the Tamar Valley. HVSR peaks from all components (HVSR, axial-HVSR and transverse-HVSR) agree well with the peak on the ellipticity curve above a layered earth (Fig. 16, top left). We observe a separation of the peaks on simulated axial-HVSR and transverse-HVSR, indication of a 2-D pattern of resonance at distance $200 \leq x \leq 400$ m from the edge of the valley. The peaks on simulated HVSR above the deepest point of the valley (Fig. 16, top right) are shifted to higher frequencies when compared to the peak on the ellipticity curve computed for an equivalent layered earth. A change in the pattern of resonance, similar to what was observed on the HVSR profiles recorded in Launceston, is observed between $x = 400$ m and $x = 500$ m, where the peak is unclear on simulated HVSR curves.

Simulated axial-HVSR and transverse-HVSR profiles are presented in Figs 17 and 18 to better identify the pattern of resonance which develops in the 2-D model representation of the Tamar Valley. The expected 1-D frequency of resonance for the equivalent layered

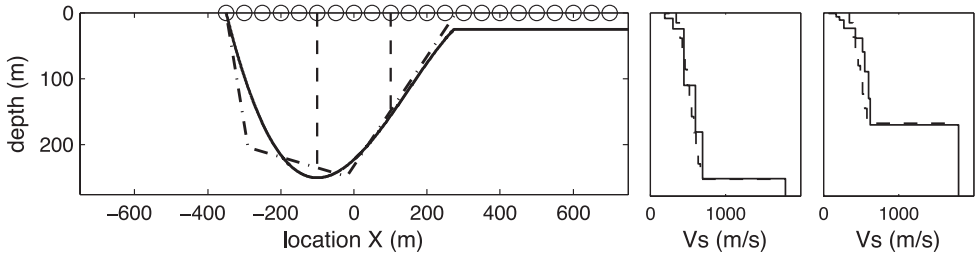

Figure 15. (a) Bedrock interface of model representation of the Tamar Valley (vertical exaggeration of 2). Circles are locations of HVSR receivers. Dash–dotted line is bedrock interface interpreted from gravity survey by Leaman (1994) (Fig. 2b, Profile #2). Dashed lines are the location of SWV profiles presented in (b) for site DBL, and (c) for site OGL. Solid lines on SWV profiles are preferred SWV profiles from SPAC observations; dashed lines are SWV approximation used for the numerical simulations of the Tamar Valley.

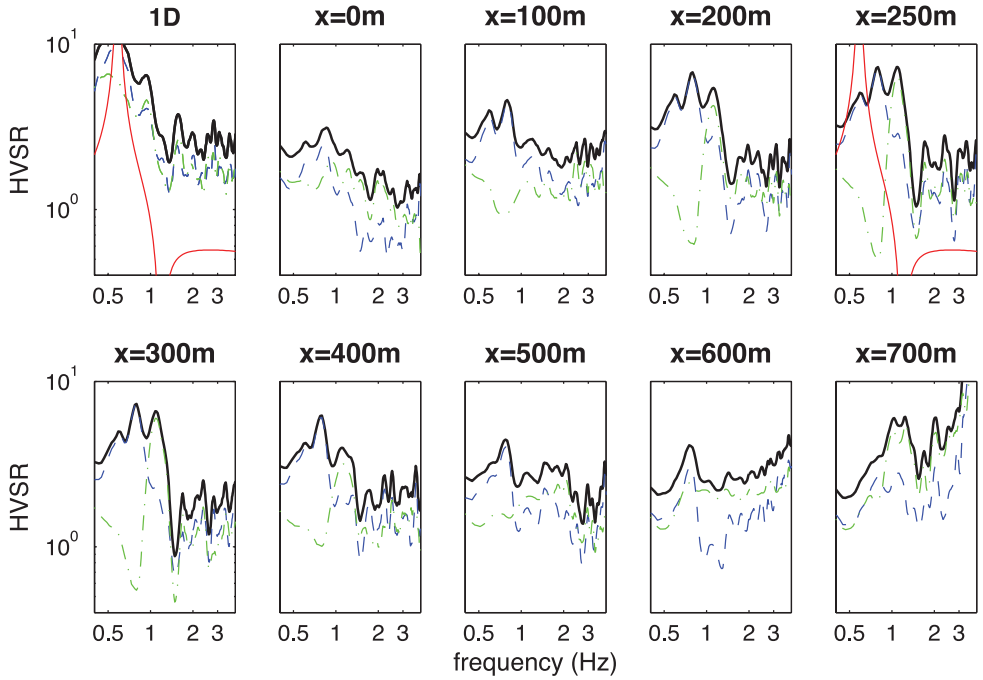

Figure 16. Simulated HVSR above layered earth model (top left) of SWV profile from Fig. 15(b); and at distance x from the left edge of the 2-D model representation of the Tamar Valley. Thick solid black line is conventional HVSR; dashed blue line is axial-HVSR; dash–dotted green line is transverse-HVSR. Solid red line is the Rayleigh wave ellipticity computed assuming a layered earth model of SWV profile from Fig. 15(b). Rayleigh wave ellipticity is presented for location where the depth to bedrock interface is simulated at $H = 250$ m.

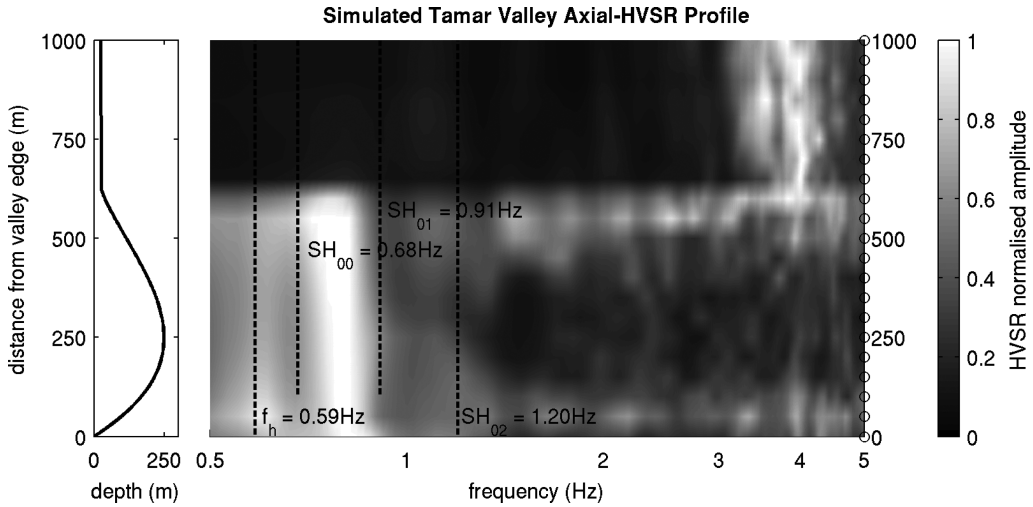

Figure 17. Simulated axial-HVSR profile across a 2-D model representation of the Tamar Valley (left). Expected frequencies of resonance f_h from Rayleigh wave ellipticity from SWV profile presented in Fig. 15(b), and f_{00}^{SH}, f_{01}^{SH} and f_{02}^{SH} computed from Bard and Bouchon's model are presented. Circles on the right are the location of HVSR observations along the profile.

earth (SWV profile from Fig. 15b) is computed at $f_h = 0.59$ Hz. No peak is detected at this frequency on the simulated axial- or transverse-HVSR profiles. Using Bard and Bouchon's model with a shape ratio $SR = 0.59$ ($H = 250$ m, $w = 421$ m), we seek to identify 2-D frequencies of resonance on the simulated HVSR profiles.

A broad peak is observed on the axial-HVSR profile at frequency $f = 0.81$ Hz, between the expected frequencies of resonance $f_{00}^{SH} = 0.68$ and $f_{01}^{SH} = 0.91$ Hz. Similar difficulties in precisely separating the multiple SH modes of resonance were recognized on the Paterson and Frankland Streets HVSR profiles. While simulated HVSR data fails to provide accurate detection of the different SH modes of resonance, it is effective in the recognition of a 2-D pattern of resonance; the peak on the axial-HVSR is located at frequency significantly higher than that of the equivalent layered earth.

The fundamental SV mode of resonance is accurately identified on the simulated transverse-HVSR profile (Fig. 18). The peak is observed at $f = 1.11$ Hz, approximately equal to the computed SV frequency of resonance $f_{fund}^{SV} = 1.17$ Hz (eq. 3). This confirms the capability of the transverse-HVSR to identify the SV mode of resonance across a deep and narrow valley such as the Tamar Valley.

The peak on the transverse-HVSR is not well defined at locations $x \geq 450$ m, for which location the peak seems to follow more closely the shape of the valley. The results of the numerical simulations agree well with SPAC and HVSR observations recorded across the

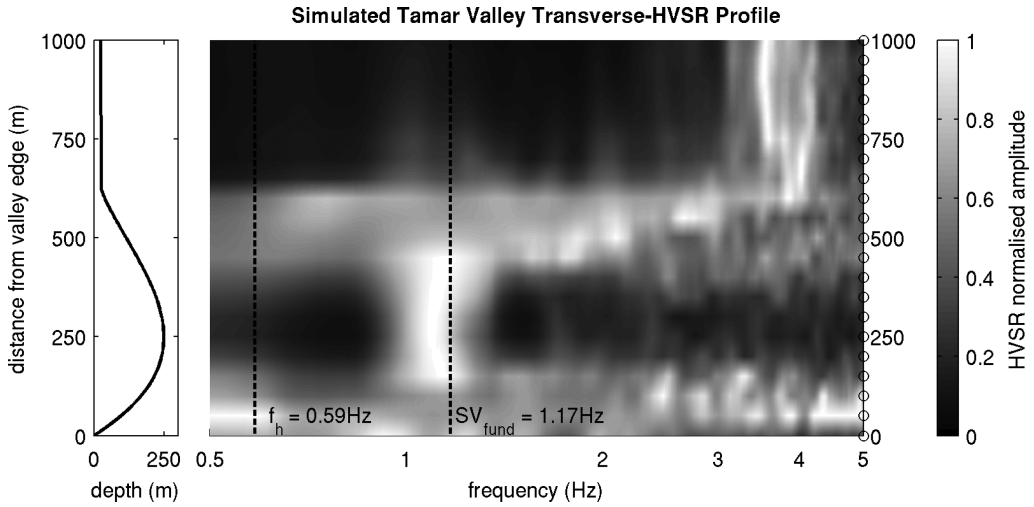

Figure 18. Simulated transverse-HVSR profile across a 2-D model representation of the Tamar Valley (left). Expected frequencies of resonance f_h from Rayleigh wave ellipticity from SWV profile in Fig. 15(b), and f^{SV}_{fund} computed from Bard and Bouchon's model are presented. Circles on the right are location of HVSR observations along the profile.

Tamar Valley in Launceston, and confirm the results of Lenti *et al.* (2009) concerning the possibility of developing a mixture of 1-D and 2-D patterns of resonance in a valley environment such as the Tamar Valley.

6.5 Frequencies of resonance

The site resonance study of Launceston is summarized in Table 1. The table lists the expected (from Bard and Bouchon's model), observed, and simulated frequencies of resonance at all five sites. The expected 1-D frequencies of resonance f_h are interpreted from the peaks in the Rayleigh wave ellipticity curves computed from the preferred SWV profiles evaluated by the SPAC method. The expected SH and SV frequencies of resonance are computed from the eqs (2) and (3) of Bard and Bouchon's model, using the shape ratios evaluated on Paterson Street and Frankland Street profiles. The frequencies of resonance identified on HVSR observations at all five sites in Launceston are indicated in brackets. The frequencies of resonance computed and identified from the numerical simulations of the Tamar Valley model are presented in the right column of the table.

The site resonance study completed in Launceston verifies the existence of a complex pattern of resonance across the city of Launceston. A 1-D pattern of resonance is recognised at sites GUN, RGB and OGL where the peaks identified on HVSR observations agree well with the peaks on Rayleigh wave ellipticity curves. This result was expected at site GUN, which was assumed to be located above a layered earth, however it is a surprising result at sites RGB and OGL which are located within the limits of the Tamar Valley. As initially expressed by Bard & Bouchon (1985) and later observed by Lenti *et al.* (2009), certain valleys simultaneously develop 1-D and 2-D patterns of resonance. We suggest this is the case in the Tamar Valley, where a 2-D pattern of resonance is clearly recognized at sites KPK and DBL, located above the deepest point of the valley.

We observe from Table 1 that HVSR observations are adequate to identify the expected frequency of resonance in a layered earth, and the expected $f^{\text{SV}}_{\text{fund}}$ frequency of resonance in valley environment. Good fits are obtained between expected and observed $f^{\text{SV}}_{\text{fund}}$ at sites KPK and DBL above the deepest point of the valley. While HVSR observations can detect the shift in frequency induced by the SH mode of resonance, they fail to identify the expected SH frequencies with adequate precision. The frequencies of resonance of the SH mode can be estimated by using the peak of the ellipticity curve determined from SPAC observations, and computing the shifts to higher frequencies from Bard and Bouchon's model. Combining the results from SPAC and HVSR methods permits to get the complete picture of the site resonance study across the Tamar Valley.

7 CONCLUSIONS

We conducted a site resonance study at five separate sites in and around the deep and narrow Tamar Valley in the City of Launceston

Table 1. Expected 1-D frequencies of resonance f_h computed on the Rayleigh wave ellipticity curves from the preferred SWV profiles, and SH and SV frequencies of resonance computed at separate sites in Launceston. Frequencies of resonance identified on HVSR observations at five sites in Launceston, and above the deepest part of model representation of the Tamar Valley are presented in brackets (frequency in Hz). The question mark '?' indicates these values are identified with low confidence on HVSR observations.

Mode	GUN	RGB	KPK	DBL	OGL	Tamar
f_h	1.16 (1.18)	1.24 (1.31)	0.74 (–)	0.61 (–)	0.95 (0.87)	0.59 (–)
SH_{00}	–	–	0.83 (–)	0.71 (–)	–	0.68 (–)
SH_{01}	–	–	1.01 (0.90)	0.94 (0.90)	–	0.91 (0.81)
SH_{02}	–	–	1.27 (1.25?)	1.24 (1.20?)	–	1.20 (–)
SV_{fund}	–	–	1.24 (1.16)	1.21 (1.18)	–	1.17 (1.11)

(Tasmania, Australia). We combine the use of the array based SPAC microtremor method to evaluate SWV profiles with single station HVSR microtremor observations to evaluate the frequency of all modes of resonance.

The SPAC method is conventionally applied to reliably evaluate the SWV profile at site GUN, located above an assumed layered earth. The frequency of resonance is identified at f_h = 1.18 Hz from HVSR observations; frequency which agrees well with the expected frequency of resonance above a layered earth from the Rayleigh wave ellipticity curve computed at site GUN.

The interpretation of SPAC observations at sites RGB and OGL provides credible SWV profiles at both sites. While the gravity survey from Leaman (1994) suggests these sites are located in an area having 2-D geology, the similar behaviour of the observed coherency spectra when comparing different orientations suggests the geology can be approximated by a layered earth at both sites. This is confirmed by HVSR observations which peaks, identified at the same frequency on the axial and transverse components, agree well with the peaks on the Rayleigh wave ellipticity curves computed from the SWV profiles interpreted by SPAC method. HVSR measurements simulated in a 2-D model representation of the Tamar Valley confirm the presence of a 1-D pattern of resonance above the flank of the valley. The frequency of resonance identified on HVSR observations is estimated at f_h = 1.31 Hz at site RGB, and at f_h = 0.87 Hz at site OGL.

A 2-D pattern of resonance is detected above the deepest part of the Tamar Valley on two HVSR profiles recorded transverse to the valley axis along Paterson and Frankland Streets, as judged from the separation of SH and SV modes of resonance at sites KPK and DBL. The fundamental SV frequency of resonance is identified on the transverse-HVSR component at f = 1.16 Hz along Paterson Street profile and at f = 1.18 Hz along Frankland Street profile. While a shift to higher frequencies is clearly recognized on both axial-HVSR profiles, HVSR observations fail to identify with precision the SH frequencies of resonance expected to develop in the Tamar Valley.

SPAC observations recorded above the deepest point of the valley are used to constrain the SWV structure and geometry of the Tamar Valley, and to evaluate the different SH modes of resonance expected to develop in the valley. As originally proposed in CAK1, coherency spectra recorded with pairs of sensors oriented parallel to the valley axis (axial-COH) are used to evaluate the SWV profile above the deepest point of the valley at site DBL.

From Bard and Bouchon's model, we can evaluate the expected SH and SV frequencies of resonance in the Tamar Valley by computing the Rayleigh wave ellipticity curve from the SWV profile evaluated by axial-COH above the deepest point of the valley. The frequencies of resonance expected to develop across the Tamar Valley along Frankland Street are f_{00}^{SH} = 0.71 Hz, f_{01}^{SH} = 0.94 Hz, f_{02}^{SH} = 1.24 Hz and $f_{\mathrm{fund}}^{\mathrm{SV}}$ = 1.21 Hz.

We suggest the frequencies of resonance are shifted to slightly higher frequencies along the Paterson Street profile, but lack of resolution of the bedrock interface with SPAC observations limits the conclusions. Observations with larger SPAC arrays would be necessary to gain resolution at depth. Deployment of such arrays was made difficult by the layout of the streets of Launceston. The best estimates of the expected frequencies of resonance along Paterson Street profile are f_{00}^{SH} = 0.83 Hz, f_{01}^{SH} = 1.01 Hz, f_{02}^{SH} = 1.27 Hz and $f_{\mathrm{fund}}^{\mathrm{SV}}$ = 1.24 Hz.

The results demonstrate a successful application of combined SPAC and HVSR observations recorded at separate sites to conduct a site resonance study in a 2-D valley environment, where the use of both methods allows identification of the complex pattern of resonance (modes and frequencies of resonance) which develops in this narrow deep valley.

ACKNOWLEDGMENTS

Maxime Claprood is supported by a Monash Graduate Scholarship, an International Postgraduate Research Scholarship, and a Québec's Funds for Nature and Technology Scholarship. Seismometers used in this project were loaned to Monash University by the Australian National Seismic Imaging Resource (ANSIR). We are grateful to the City Council of Launceston, for their assistance during field survey. Geological maps of Launceston were provided by Mineral Resources Tasmania. We would like to recognize the help of Miss Janett Steiner for her assistance during the field survey. Thanks are due to the editor Prof. Jean Virieux and Matteo Picozzi whose constructive suggestions helped improving the quality of the manuscript and our research in general.

REFERENCES

Aki, K., 1957. Space and time spectra of stationary stochastic waves, with special reference to microtremors, *Bull. Earthq. Res. Inst.*, **35**, 415–456.

Arai, H. & Tokimatsu, K., 2005. S-wave velocity profiling by joint inversion of microtremor dispersion curve and horizontal-to-vertical (H/V) spectrum, *Bull. seism. Soc. Am.*, **95**(5), 1766–1778, doi:10.1785/0120040243.

Asten, M., 2006a. On bias and noise in passive seismic data from finite circular array data processed using SPAC methods, *Geophysics*, **71**(6), V153–V162, doi:10.1190/1.2345054.

Asten, M., 2006b. Site shear velocity profile interpretation from microtremor array data by direct fitting of SPAC curves, in *Proceedings of the Third Int. Symp. Effects of Surface Geol. Seismic Motion*, Vol. 2, LCPC Editions, Grenoble, France, August 30–September 01, Paper No. 99, pp. 1069–1080.

Asten, M., Lam, N., Gibson, G. & Wilson, J., 2002. Microtremor survey design optimised for application to site amplification and resonance modelling, in *Proceedings of Conference on Total Risk Management in the Privatised Era*, Australian Earthquake Engineering Society, Adelaide, Australia, Paper No. 7.

Asten, M., Dhu, T. & Lam, N., 2004. Optimised array design for microtremor array studies applied to site classification; comparison of results with SCPT logs, in *Proceedings of the 13th World Conf. Earthq. Eng.*, Vancouver, Canada, Paper No. 2903.

Bard, P.-Y. & Bouchon, M., 1980a. The seismic response of sediment-filled valleys. Part 1. The case of incident SH waves, *Bull. seism. Soc. Am.*, **70**(4), 1263–1286.

Bard, P.-Y. & Bouchon, M., 1980b. The seismic response of sediment-filled valleys. Part 2. The case of incident P and SV waves, *Bull. seism. Soc. Am.*, **70**(5), 1921–1941.

Bard, P.-Y. & Bouchon, M., 1985. The two-dimensional resonance of sediment-filled valleys, *Bull. seism. Soc. Am.*, **75**(2), 519–541.

Barnaba, C., Marello, L., Vuan, A., Palmieri, F., Romanelli, M., Priolo, E., & Braitenberg, C., 2010. The buried shape of an alpine valley from gravity surveys, seismic and ambient noise analysis, *Geophys. J. Int.*, **180**, 715–733.

Capon, J., 1973. Signal processing and frequency-wavenumber spectrum analysis for a large aperture seismic array, *Methods in Computational Physics*, Vol. 13, Academic Press Inc., New York, NY.

Cara, F. *et al.*, 2008. Microtremor measurements in the City of Palermo, Italy: Analysis of the correlation between local geology and damage, *Bull. seism. Soc. Am.*, **98**(3), 1354–1372.

Chávez-García, F. & Rogríguez, M., 2007. The correlation of microtremors: empirical limits and relations between results in frequency and time domains, *Geophys. J. Int.*, **171**, 657–664, doi:10.1111/j.1365-246X.2007.03529.x.

Chávez-García, F., Rodríguez, M. & Stephenson, W., 2005. An alternative approach to the SPAC analysis of microtremors: exploiting stationarity of noise, *Bull. seism. Soc. Am.*, **95**(1), 277–293, doi:10.1785/0120030179.

Chávez-García, F., Domínguez, T., Rodríguez, M. & Pérez, F., 2007. Site effects in a volcanic environment: A comparison between HVSR and array techniques at Colima, Mexico, *Bull. seism. Soc. Am.*, **97**(2), 591–604, doi:10.1785/0120060095.

Claprood, M. & Asten, M., 2008a. Comparison of array microtremor survey methods for estimation of dispersion curves in Launceston, Australia, in *Symposium on the Application of Geophysics to Engineering and Environmental Problems (SAGEEP)*, Environmental and Engineering Geophysical Society, Philadelphia, PA.

Claprood, M. & Asten, M., 2008b. Microtremor survey methods in the Tamar Valley, Launceston, Tasmania: Evidence of 2D resonance from microtremor observations, in *Proceedings of the Earthq. Eng. Australia 2008 Conference*, Australian Earthquake Engineering Society, Ballarat, Australia, Paper No. 20.

Claprood, M. & Asten, M., 2010. Statistical validity control on SPAC microtremor observations recorded with a restricted number of sensors, *Bull. seism. Soc. Am.*, **100**(2), 776–791, doi:10.1785/0120090133.

Claprood, M., Asten, M. & Kristek, J., 2011. Using the SPAC microtremor method to identify 2D effects and evaluate 1D shear-wave velocity profile in valleys, *Bull. seism. Soc. Am.*, **101**(2).

Cornou, C., Bard, P.-Y. & Dietrich, M., 2003a. Contribution of dense array analysis to the identification and quantification of basin-edge-induced waves, Part I: Methodology, *Bull. seism. Soc. Am.*, **93**(6), 2604–2623.

Cornou, C., Bard, P.-Y. & Dietrich, M., 2003b. Contribution of dense array analysis to the identification and quantification of basin-edge-induced waves, Part II: Application to Grenoble Basin (French Alps), *Bull. seism. Soc. Am.*, **93**(6), 2624–2648.

Di Giulio, G., Cornou, C., Ohrnberger, M., Wathelet, M. & Rovelli, A., 2006. Deriving wavefield characteristics and shear-velocity profiles from two-dimensional small-aperture arrays analysis of ambient vibrations in a small-size alluvial basin, Colfiorito, Italy, *Bull. seism. Soc. Am.*, **96**(5), 1915–1933, doi:10.1785/0120060119.

Di Giulio, G. *et al.*, 2012. Exploring the model space and ranking a best class of models in surface-wave dispersion inversion: application at European string-motion sites, *Geophysics*, **77**(3), B147–B166.

Dravinski, M., Ding, G. & Wen, K.-L., 1996. Analysis of spectral ratios for estimating ground motion in deep basins, *Bull. seism. Soc. Am.*, **86**(3), 646–654.

Ekström, G., Abers, G. & Webb, S., 2009. Determination of surface-wave phase velocities across USArray from noise and Aki's spectral formulation, *Geophys. Res. Lett.*, **36**, L18301, doi:10.1029/2009GL039131.

Fäh, D., Kind, F. & Giardini, D., 2003. Inversion of local S-wave velocity structures from average H/V ratios, and their use for the estimation of site-effects, *J. Seismol.*, **7**, 449–467.

Fäh, D., Stamm, G. & Havenith, H.-B., 2008. Analysis of three-component ambient vibration array measurements, *Geophys. J. Int.*, **172,** 199–213, doi:10.111/j.1365-246X.2007.03625.x.

Field, E., 1996. Spectral amplification in a sediment-filled valley exhibiting clear basin-edge-induced waves, *Bull. seism. Soc. Am.*, **86**(4), 991–1005.

Field, E. & Jacob, K., 1995. A comparison and test of various site-response estimation techniques, including three that are not reference-site dependent, *Bull. seism. Soc. Am.*, **85**(4), 1127–1143.

Frischknecht, C. & Wagner, J.-J., 2004. Seismic soil effect in an embanked deep alpine valley: a numerical investigation of two-dimensional resonance, *Bull. seism. Soc. Am.*, **94**(1), 171–186.

Hartzell, S., Carver, D., Williams, R., Harmsen, S. & Zerva, A., 2003. Site response, shallow shear-wave velocity, and wave propagation at the San Jose, California, dense seismic array, *Bull. seism. Soc. Am.*, **93**(1), 443–464.

Henstridge, J., 1979. A signal processing method for circular arrays, *Geophysics*, **44**(2), 179–184.

Herrmann, R., 2002. *Computer programs in seismology: An overview of synthetic seismogram computation*, Saint Louis University, MO, version 3.30.

Hinzen, K.-G., Weber, B. & Scherbaum, F., 2004. On the resolution of H/V measurements to determine sediment thickness, a case study across a normal fault in the Lower Rhine Embayment, Germany, *J. Earthq. Eng.*, **8**(6), 909–926.

Horike, M., 1985. Inversion of phase velocity of long-period microtremors to the s-wave velocity structure down to the basement in urbanized areas, *J. Phys. Earth*, **33**, 59–96.

Ibs-von Seht, M. & Wohlenberg, J., 1999. Microtremor measurements used to map thickness of soft sediments, *Bull. seism. Soc. Am.*, **89**(1), 250–259.

Kawase, H. & Aki, K., 1989. A study on the response of a soft basin for incident S, P, and Rayleigh waves with special references to the long duration observed in Mexico City, *Bull. seism. Soc. Am.*, **79**(5), 1361–1382.

Köhler, A., Ohrnberger, M., Scherbaum, F., Wathelet, M. & Cornou, C., 2007. Assessing the reliability of the modified three-component spatial autocorrelation technique, *Geophys. J. Int.*, **168**, 779–796, doi:10.1111/j.1365-246X.2006.03253.x.

Kristek, J., Moczo, P. & Archuleta, R., 2002. Efficient methods to simulate planar free surface in the 3D 4th-order staggered grid finite-difference schemes, *Stud. Geophys. Geod.*, **46**, 355–381.

Kristek, J., Moczo, P. & Pazak, P., 2006. Numerical modeling of earthquake motion in Grenoble Basin, France, using a 4th-order velocity-stress arbitrary discontinuous staggered-grid FD scheme, in *Proceedings of the Third Int. Symp. Effects of Surface Geol. Seism. Motion*, vol. 2, LCPC Editions, Grenoble, France, August 30–September 01.

Kudo, K. *et al.*, 2002. Site-specific issues for strong ground motions during the Kocaeli, Turkey, earthquake of 17 August 1999, as inferred from array observations of microtremors and aftershocks, *Bull. seism. Soc. Am.*, **92**(1), 448–465.

Lachet, C. & Bard, P.-Y., 1994. Numerical and theoretical investigations on the possibilities and limitations of Nakamura's technique, *J. Phys. Earth*, **42**, 377–397.

Leaman, D., 1994. Assessment of gravity survey City of Launceston, Technical Report, Leaman Geophysics, Hobart, Tasmania, Australia, for Launceston City Corporation Seismic Zonation Study.

Lenti, L., Martino, S., Paciello, A. & Scarascia Mugnozza, G., 2009. Evidence of two-dimensional amplification effects in an alluvial valley (Valnerina, Italy) from velocimetric records and numerical models, *Bull. seism. Soc. Am.*, **99**(3), 1612–1635, doi:10.1785/0120080219.

Michael-Leiba, M., 1995. Microtremor survey and seismic microzonation Launceston, Tasmania, Technical Report, Australian Geological Survey, Canberra, ACT, Australia, for Launceston City Council.

Mirzaoglu, M. & Dýkmen, U., 2003. Application of microtremors to seismic microzoning procedure, *J. Balkan Geophys. Soc.*, **6**(3), 143–156.

Moczo, P. & Kristek, J., 2002. FD code to generate noise synthetic, Technical Report D02.09, European Commission: Research General Directorate, Project No. EVG1-CT-2000-00026, SESAME. Available at: http://sesame-fp5.obs.ujf-grenoble.fr [last accessed 2006].

Moczo, P., Kristek, J., Vavryčuk, V., Archuleta, R. & Halada, L., 2002. 3D heterogeneous staggered-grid finite-difference modeling of seismic motion with volume harmonic and arithmetic averaging of elastic moduli and densities, *Bull. seism. Soc. Am.*, **92**(8), 3042–3066.

Moczo, P., Robertsson, J. & Eisner, L., 2007. The finite-difference time-domain method for modeling of seismic wave propagation, *Advances in Geophys.*, **48**, 421–516, doi:10.1016/S0065-2687(06)48008-0.

Morikawa, H., Sawada, S. & Akamatsu, J., 2004. A method to estimate phase velocities of Rayleigh waves using microseisms simultaneously observed at two sites, *Bull. seism. Soc. Am.*, **94**(3), 961–976.

Nakamura, Y., 1989. A method for dynamic characteristics estimation of subsurface using microtremor on the ground surface, *Quarterly Report of Railway Technical Research Institute*, **30**, 25–33.

Nogoshi, M. & Igarashi, T., 1971. On the amplitude characteristics of microtremor, Part II, *J. Seismol. Soc. Japan*, **24**, 26–40.

Okada, H., 2003. *The Microtremor Survey Method*, Geophysical Monograph Series No. 12, Society of Exploration Geophysicists, Tulsa, OK.

Okada, H., 2006. Theory of efficient array observations of microtremors with special reference to the SPAC method, *Exploration Geophys.*, **37**(1), 73–85.

Paolucci, R., 1999. Shear resonance frequencies of alluvial valleys by Rayleigh's method, *Earthq. Spectra*, **15**(3), 503–521.

Parolai, S., Bormann, P. & Milkereit, C., 2002. New relationships between Vs, thickness of sediments, and resonance frequency calculated by the H/V ratio of seismic noise for the Cologne area (Germany), *Bull. seism. Soc. Am.*, **92**(6), 2521–2527.

Parolai, S., Picozzi, M., Richwalski, M. & Milkereit, C., 2005. Joint inversion of phase velocity dispersion and H/V ratio curves from seismic noise recordings using a genetic algorithm, considering higher modes, *Geophys. Res. Lett.*, **32**, L01303, doi:10.1029/2004GL021115.

Picozzi, M., Parolai, S. & Albarello, D., 2005. Statistical analysis of noise horizontal-to-vertical spectral ratios (HVSR), *Bull. seism. Soc. Am.*, **95**(5), 1779–1786, doi:10.1785/0120040152.

Picozzi, M., Strollo, A., Parolai, S., Durukal, E., Özel, O., Karabulut, S., Zschau, J. & Erdik, M., 2009. Site characterization by seismic noise in Istanbul, Turkey, *Soil Dyn. Earthq. Eng.*, **29**, 469–482, doi:10.1016/j.soildyn.2008.05.007.

Roten, D. & Fäh, D., 2007. A combined inversion of Rayleigh wave dispersion and 2-D resonance frequencies, *Geophys. J. Int.*, **168**, 1261–1275, doi:10.1111/j.1365-246X.2006.03260.x.

Roten, D., Fäh, D., Cornou, C. & Giardini, D., 2006. Two-dimensional resonances in Alpine valleys identified from ambient vibration wavefields, *Geophys. J. Int.*, **165**, 889–905.

Roten, D., Fäh, D., Olsen, K. & Giardini, D., 2008. A comparison of observed and simulated site response in the Rhône valley, *Geophys. J. Int.*, **173**, 958–978, doi:10.1111/j.1365-246X.2008.03774.x.

Satoh, T., Kawase, H., Iwata, T., Higashi, S., Sato, T., Irikura, K. & Huang, H.-C., 2001. S-wave velocity structure of the Taichung Basin, Taiwan, estimated from array and single-station records of microtremors, *Bull. seism. Soc. Am.*, **91**(5), 1267–1282.

Scherbaum, F., Hinzen, K.-G. & Ohrnberger, M., 2003. Determination of shallow shear wave velocity profiles in the Cologne, Germany area using ambient vibrations, *Geophys. J. Int.*, **152**, 597–612.

Steimen, S., Fäh, D., Kind, F., Schmid, C. & Giardini, D., 2003. Identifying 2D resonance in microtremor wave fields, *Bull. seism. Soc. Am.*, **93**(2), 583–599.

Tanimoto, T. & Alvizuri, C., 2006. Inversion of the HZ ratio of microseisms for S-wave velocity in the crust, *Geophys. J. Int.*, **165**, 323–335, doi:10.1111/j.1365-246X.2006.02905.x.

Tokimatsu, K., 1997. Geotechnical site characterization using surface waves, in *Earthquake Geotechnical Engineering: Proceedings IS-Tokyo 95,* 1st International Conf. on Earthquake Geotechnical Engineering, pp. 1333–1368, ed. Ishihara, K.

Uebayashi, H., 2003. Extrapolation of irregular subsurface structures using the horizontal-to-vertical spectral ratio of long-period microtremors, *Bull. seism. Soc. Am.*, **93**(2), 570–582.